THE JOURNAL OF BIOLOGICAL CHEMISTRY VOL. 291, NO. 42, pp. 21857–21868, October 14, 2016

The N Terminus of the Prion Protein Mediates Functional Interactions with the Neuronal Cell Adhesion Molecule (NCAM) Fibronectin Domain*[S]

Received for publication, June 13, 2016, and in revised form, August 10, 2016 Published, JBC Papers in Press, August 17, 2016, DOI 10.1074/jbc.M116.743435

Urška Slapšak[‡], Giulia Salzano[§], Ladan Amin[§], Romany N. N. Abskharon[¶‖], Gregor Ilc[‡ ‡‡], Blaž Zupančič[‡], Ivana Biljan[§§], Janez Plavec[‡ ‡‡¶¶1], Gabriele Giachin[§‖‖], and Giuseppe Legname[§2]**

*From the [‡]Slovenian NMR Centre, National Institute of Chemistry, Hajdrihova 19, SI-1000 Ljubljana, Slovenia, the [§]Laboratory of Prion Biology, Department of Neuroscience, Scuola Internazionale Superiore di Studi Avanzati (SISSA), Via Bonomea 265, Trieste I-34136, Italy, the [¶]Structural Biology Research Center, Vrije Universiteit Brussel, VIB, Pleinlaan 2, 1050, Brussels, Belgium, the [‡‡]EN-FIST Centre of Excellence, Dunajska 156, SI-1000 Ljubljana, Slovenia, the [§§]Department of Chemistry, Faculty of Science, University of Zagreb, Horvatovac 102A, Zagreb HR-10000, Croatia, the [¶¶]Department of Chemistry and Biochemistry, Faculty of Chemistry and Chemical Technology, University of Ljubljana, Večna pot 113, SI-1000 Ljubljana, Slovenia, the [‖‖]Structural Biology Group, European Synchrotron Radiation Facility (ESRF), 71 Avenue des Martyrs, 38000-Grenoble, France, the [‖]National Institute of Oceanography and Fisheries (NIOF), 11516 Cairo, Egypt, and the **Van Andel Research Institute, Grand Rapids, Michigan 49503*

The cellular form of the prion protein (PrP^C) is a highly conserved glycoprotein mostly expressed in the central and peripheral nervous systems by different cell types in mammals. A misfolded, pathogenic isoform, denoted as prion, is related to a class of neurodegenerative diseases known as transmissible spongiform encephalopathy. PrP^C function has not been unequivocally clarified, and it is rather defined as a pleiotropic protein likely acting as a dynamic cell surface scaffolding protein for the assembly of different signaling modules. Among the variety of PrP^C protein interactors, the neuronal cell adhesion molecule (NCAM) has been studied *in vivo*, but the structural basis of this functional interaction is still a matter of debate. Here we focused on the structural determinants responsible for human PrP^C (HuPrP) and NCAM interaction using stimulated emission depletion (STED) nanoscopy, SPR, and NMR spectroscopy approaches. PrP^C co-localizes with NCAM in mouse hippocampal neurons, and this interaction is mainly mediated by the intrinsically disordered PrP^C N-terminal tail, which binds with high affinity to the NCAM fibronectin type-3 domain. NMR structural investigations revealed surface-interacting epitopes governing the interaction between HuPrP N terminus and the second module of the NCAM fibronectin type-3 domain. Our data provided molecular details about the interaction between HuPrP and the NCAM fibronectin domain, and revealed a new role of PrP^C N terminus as a dynamic and functional element responsible for protein-protein interaction.

A misfolded form of the host-encoded cellular prion protein (PrP^C)[3] is the causative agent for a class of human and animal neurodegenerative diseases denoted as transmissible spongiform encephalopathies. PrP^C is a sialoglycoprotein, tethered to the outer leaflet of the plasma membrane by a glycosylphosphatidylinositol (GPI) anchor. Soluble, natively α-helix-folded monomers of PrP^C may adopt an aggregated protease-resistant conformation known as PrP^{Sc} (1). The mature human PrP^C (HuPrP) is composed of 209 residues including a largely unstructured N-terminal part and a globular α-helix-rich C-terminal domain (2). Conversely, PrP^{Sc} is β-sheet-enriched, partially protease-resistant, insoluble, and multimeric (3). The insoluble nature of PrP^{Sc} and its propensity to aggregate have hampered the use of high-resolution techniques, and therefore different PrP^{Sc} models currently exist (4).

Despite the fact that PrP^C is highly conserved among different species, its physiological function has not been fully clarified. Defining PrP^C function remains one of the main challenges in prion biology, and it is also an absolute requirement for understanding prion diseases. It is now being accepted that PrP^C is a pivotal molecule with diverse roles in brain development and in neural plasticity in the adult (5–8). Proposed PrP^C functions range from neuronal growth and differentiation (9), synaptic plasticity (10, 11), cell signaling (12,

* This work was supported by the EC through FP7 222887 "Priority" (to G. L.). This work was also supported by a fellowship from the S.H.A.R.M. project (Supporting Human Assets in Research and Mobility, funded by the Friuli Venezia Giulia autonomous Region (Italy) through the Operational Program of the European Social Fund 2007/2013; Grant agreement number FP1123744003) (to G. G.), and by the Slovenian Research Agency (ARRS) Grant P1-242. The authors declare that they have no conflicts of interest with the contents of this article.

[S] This article contains supplemental Figs. S1 and S2.

The atomic coordinates and structure factors (code 5LKN) have been deposited in the Protein Data Bank (http://wwpdb.org/).

[1] To whom correspondence may be addressed: Slovenian NMR Centre, National Institute of Chemistry, Hajdrihova 19, SI-1000 Ljubljana, Slovenia. E-mail: janez.plavec@ki.si.

[2] To whom correspondence may be addressed: Laboratory of Prion Biology, Dept. of Neuroscience, Scuola Internazionale Superiore di Studi Avanzati (SISSA), Via Bonomea 265, Trieste I-34136, Italy. E-mail:: legname@sissa.it.

[3] The abbreviations used are: PrP, prion protein; HuPrP, human prion protein; MoPrP, mouse prion protein; BCL, short peptide from neuronal cell adhesion molecule; FNIII1,2, two fibronectin type-3 domains; FNIII1, first module of fibronectin type-3 domain; FNIII2, second module of fibronectin type-3 domain; NCAM, neuronal cell adhesion molecule; GAG, glycosaminoglycan; GPI, glycosylphosphatidylinositol; GC, growth cone(s); STED, stimulated emission depletion nanoscopy; HSQC, heteronuclear single quantum correlation; TOCSY, total correlation spectroscopy; RMSD, root mean square deviation.

13), NMDA receptor regulation (14, 15), and brain metal homeostasis (16). Putative functions are based on PrP^C-interacting molecules present on the cell surface, such as the 37-kDa/67-kDa laminin receptor, the stress-inducible protein 1, and vitronectin (17–19). Among the different PrP^C protein interactors, the neuronal cell adhesion molecule (NCAM) has been extensively characterized *in vitro*, in cell-based assays, and *in vivo* (13, 20–23).

NCAM belongs to Ig superfamily cell adhesion molecules (CAMs), and it is present on the cell surface of neurons, astrocytes, and oligodendrocytes, where it mediates homophilic and heterophilic cell adhesion (24). NCAM is involved in neuronal migration, axon growth, and guidance, as well as in synaptic plasticity associated with learning and memory (25). Alternative splicing of the *NCAM1* gene results in isoforms of three size classes that differ in their membrane attachment and cytosolic regions: NCAM-180, NCAM-140 (with intracellular domains consisting of 386 and 120 amino acids, respectively), and NCAM-120 (lacking the intracellular domain and linked to the membrane by a GPI anchor). NCAM isoforms share an extracellular domain consisting of five Igs and two fibronectin type-3 (FNIII1,2) domains. Variable use of alternative exons in the extracellular domain results in small insertions into Ig4 or between the FNIII1,2 domains. NCAM function is further regulated by an unusual posttranslational modification consisting of the addition of polysialic acid to Ig5 (26, 27). Although a complete picture has yet to emerge, it appears that NCAM physiological function is mediated by multiple modes of homophilic interaction through the NCAM Ig domains (28). Additionally, NCAM is also engaged in heterophilic interactions, *i.e.* NCAM can bind other protein partners modulating different functions. Different groups have investigated the structural and molecular basis governing the interaction between the NCAM FNIII1,2 domain and the fibroblast growth factor receptor 1 (FGFR1) (29, 30).

Besides the interaction with FGFR1, NCAM can bind PrP^C and engages different cellular responses. PrP^C-NCAM binding induces NCAM redistribution in lipid rafts, leading to FYN tyrosine kinase activation and neurite outgrowth (13). ELISA experiments using an NCAM-derived peptide library against the recombinant full-length mouse prion protein (MoPrP) have shown that the FNIII1,2 domain shares highest affinity for MoPrP (21). As revealed by *in situ* cross-linking of MoPrP deletion mutants expressed in cell models, the PrP^C-binding site seems to be formed by the N terminus and a segment comprising α-helix 1 (21). However, PrP^C-NCAM interacting surfaces have not been described at the structural and biophysical levels yet. Recently, it has been observed that PrP^C controls polysialylation of NCAM during cellular morphogenesis (23). Current evidence strengthens the hypothesis that the FNIII1,2 domain plays a role for NCAM-mediated heterophilic interaction; therefore this domain may represent a useful model for structural studies aiming at understanding the molecular determinants of PrP^C-NCAM interaction.

Here we have performed cell biology, biophysical, and structural investigations on the interaction between the FNIII1,2 domain and HuPrP. Despite the inherent structural disorder of the PrP^C N-terminal domain, which can mediate its interaction with both metals and cellular polyanions (*e.g.* sulfate proteoglycans) (31), binding with physiological protein partners has not been proved yet. HuPrP segments that are able to interact with the FNIII1,2 domain were identified by SPR experiments. NMR chemical shift perturbation experiments allowed us to identify binding sites on the FNIII1,2 domain involved in the interaction with the HuPrP. The module 2 (FNIII2) of the fibronectin type-3 domain and peptides covering different parts of the HuPrP were employed as a model system. Additionally, we examined the effect of a pathological amino acid substitution, P102L, the prototypical mutation linked to a genetic form of human prion disease denoted as Gerstmann-Straussler-Scheinker disease (GSS), on binding to FNIII2. Interestingly, this mutation also unveiled a new hidden binding site corresponding to the non-octarepeat copper-binding site (32). These results may provide a structural understanding of the interaction of NCAM with PrP^C and where the binding site is located. Besides, the novel insight of the effect of HuPrP bearing the pathogenic point mutation P102L on its interaction with the FNIII2 domain is introduced here.

Results

NCAM Co-localizes with PrP^C—Functional interactions of PrP^C with its binding partner(s) have been suggested previously (13): *cis* and *trans* interactions between NCAM and PrP^C promote neurite outgrowth, and the disruption of these interactions indicates that PrP^C is involved in nervous system development cooperating with NCAM as a signaling receptor.

In this study, we used stimulated emission depletion (STED) nanoscopy to confirm the association between PrP^C and NCAM in mouse hippocampal culture. We determined simultaneously the cellular distribution of PrP^C, NCAM, and actin (Fig. 1*A*). PrP^C and NCAM share very similar distributions along the neurite and in hippocampal growth cones (GC). The staining for PrP^C and NCAM was preferentially localized in the central domain and transition zone of the GC membrane (Fig. 1*A*, *arrows*). By using STED nanoscopy, we were able to detect very low co-localization between PrP^C and NCAM, whereas treatment with 1 μM nerve growth factor (NGF) results in increased co-localization (Fig. 1*B*). The observed higher association between PrP^C and NCAM in treated cultures suggested that these proteins might functionally cooperate to transduce signals into the cell interior, which in turn trigger the neurite growth.

FNIII1,2 Domain Binds to HuPrP N-terminal Domain with High Affinity—SPR experiments were used to analyze the binding of the FNIII1,2 domain to different HuPrP and MoPrP constructs, including full-length HuPrP and MoPrP (*i.e.* from residues 23 to 231 and 23 to 230, respectively), the HuPrP N-terminal domain (residues 23–144), and the truncated C-terminal HuPrP and MoPrP (residues 90–231 and 89–230, respectively). We observed strong interaction between the FNIII1,2 domain and the HuPrP N-terminal domain with K_d of 5.4 nM. Also the full-length HuPrP binds to the FNIII1,2 domain (K_d of 337 nM), whereas for the truncated HuPrP, we were not able to report any interaction. The full-length MoPrP displayed a weak affinity for the FNIII1,2 domain (K_d 3.8 μM), whereas the truncated MoPrP behaved almost iden-

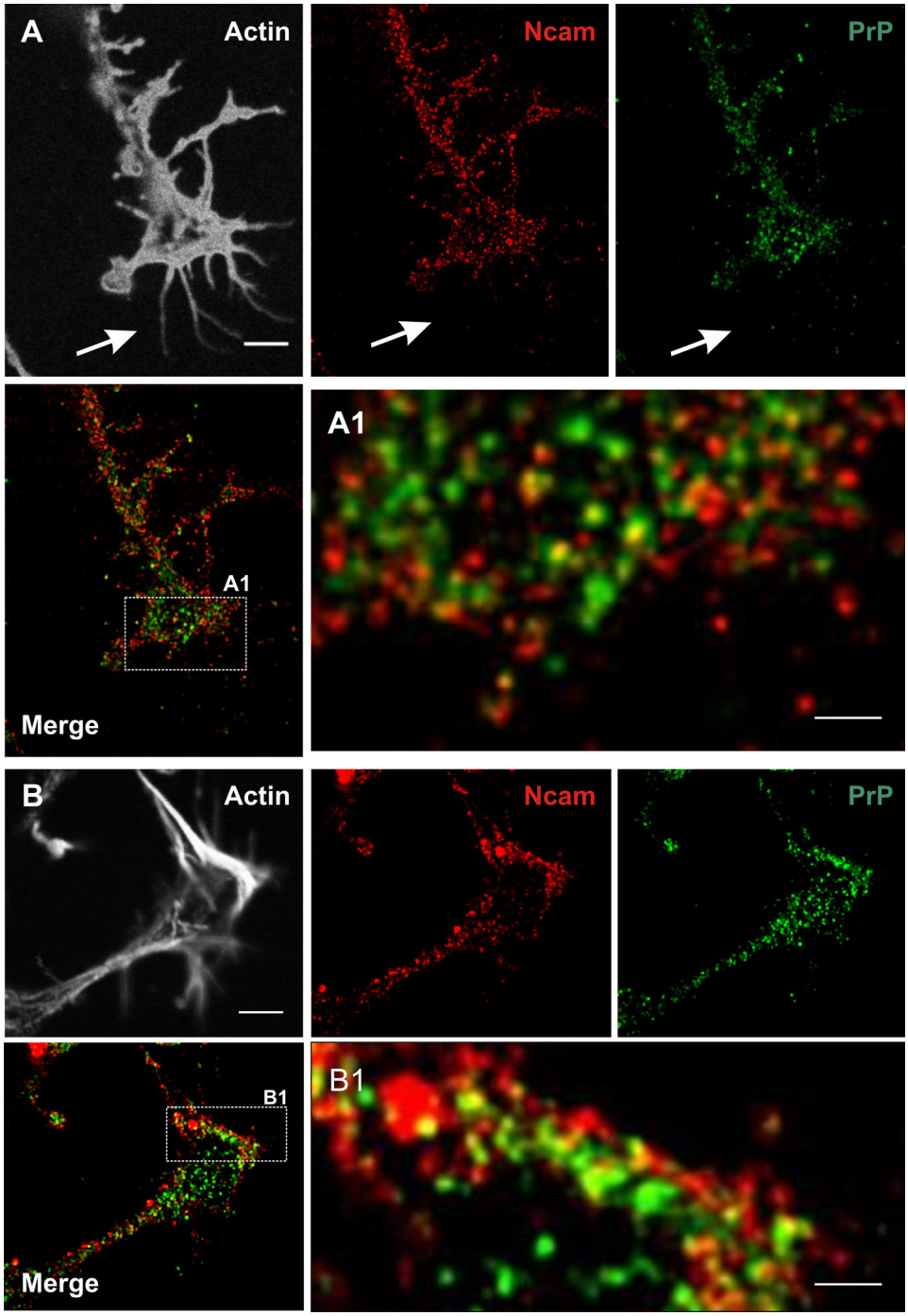

FIGURE 1. **PrP-NCAM interaction *in vitro*.** *A*, STED images of GC stained for PrP, NCAM, and actin, and merge of the PrP and NCAM in control condition. *Scale bar*, 500 nm. *A1* and *A2*, high-resolution images of areas indicated in *A*. *Scale bar*, 250 nm. *B*, as in *A*, except that neurons were incubated with 1 μM NGF (2 h).

TABLE 1

Dissociation constants for the interaction between FNIII (immobilized) and different HuPrP and MoPrP constructs

NA, not applicable.

Protein	K_d	K_{on}	K_{off}
	nM	*1/ms*	*1/s*
HuPrP(23–231)	337	2.00E+05	0.0674
HuPrP(90–231)	NA	NA	NA
HuPrP(23–144)	5.4	1.42E+06	7.66E-03
MoPrP(23–230)	3800	2.58E+04	0.0983
MoPrP(89–230)	NA	NA	NA

tically to the truncated HuPrP, displaying no interaction with the FNIII1,2 domain (Table 1 and Fig. 2). Additionally, we confirmed that a short NCAM peptide, named BCL, corresponding to the sequence of residues 620–635 in the FNIII1,2 domain, is able to interact with HuPrP using ELISA (Fig. 3). Peptide BCL also binds to MoPrP (21), and it is considered an NCAM mimetic peptide employed as NCAM surrogate in pharmacological experiments (34). These data add more insights about the HuPrP regions involved in the

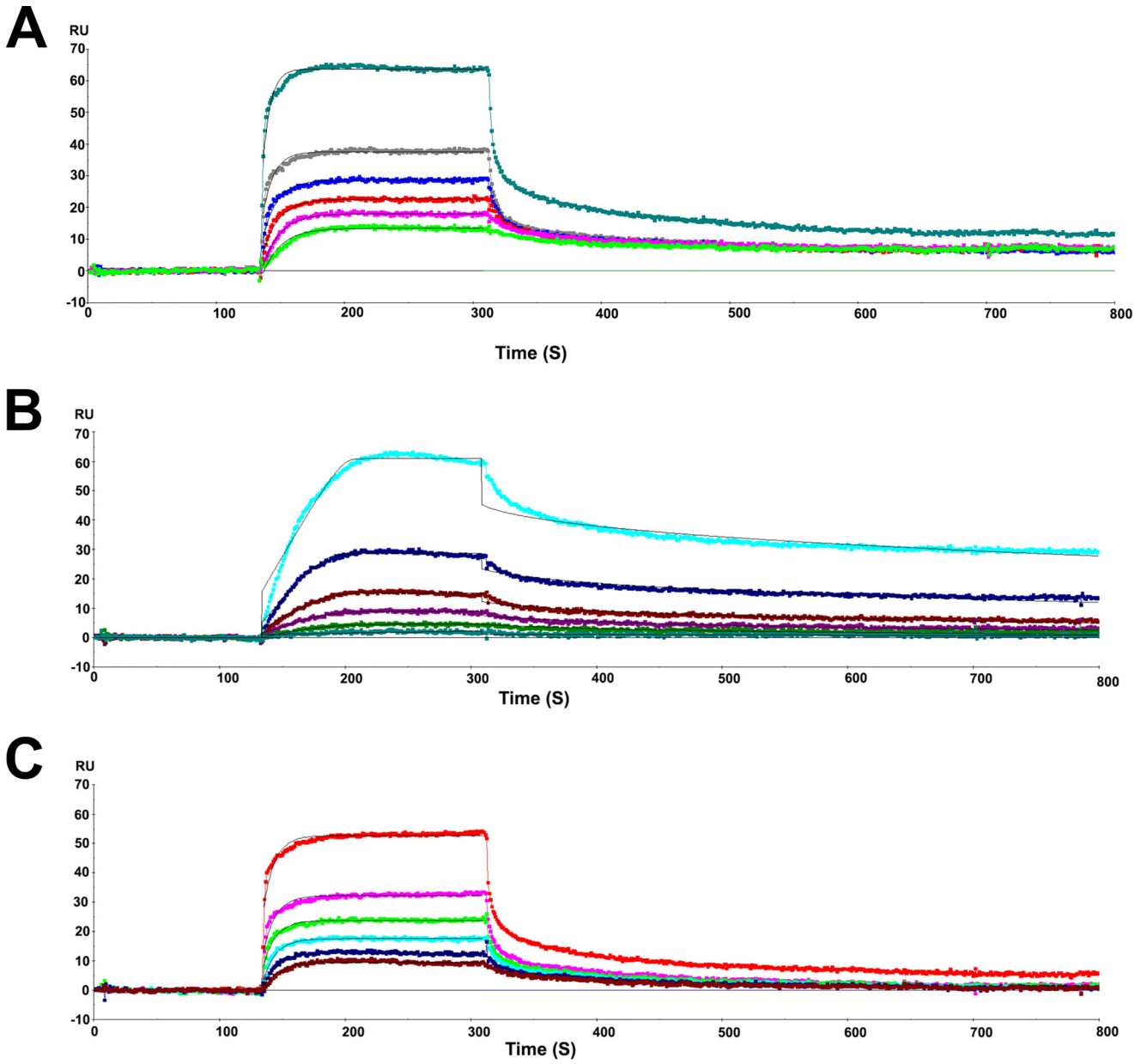

FIGURE 2. **SPR analysis of the FNIII-HuPrP or MoPrP interactions.** Shown are raw sensorgrams obtained on a Biacore 2000 instrument. Selected curves are labeled with the respective analyte concentration. *A–C*, the binding of full-length HuPrP (*A*), HuPrP N terminus (*B*), and full-length MoPrP (*C*) to immobilized FNIII. *RU*, response units.

interaction with the FNIII1,2 domain, showing that this binding is largely mediated by the unstructured N-terminal HuPrP domain.

FNIII2 Domain Was Used for NMR Characterization of Binding between HuPrP and NCAM—NMR spectroscopy is an excellent tool to evaluate and characterize the binding properties of HuPrP and NCAM in solution at atomic level. Unambiguous assignment of HuPrP(23–144) residues was not possible because of high signal overlap in the ^{15}N HSQC spectrum, which was due to the high percentage of glycine residues, octarepeats, and intrinsically disordered properties of the unstructured N terminus (supplemental Fig. S1*A*). Thus, we focused of the HuPrP interaction partner instead. ^{15}N,^{13}C-labeled FNIII1 and FNIII2 domains of NCAM were produced to find a suitable candidate for the evaluation of HuPrP-NCAM binding properties. The ^{15}N HSQC spectra of the FNIII1,2 (supplemental Fig. S1, *B–D*), FNIII1, and FNIII2 (Fig. 4) domains were recorded. The FNIII1,2 and FNIII1 domains did not exhibit suitable NMR properties for further analysis, whereas for the FNIII2 segment (with a molecular mass of 11.8 kDa), a complete NMR analysis has been carried out.

The ^{15}N HSQC spectrum of the FNIII2 domain demonstrated good dispersion of cross-peaks, indicating the potential for detailed structure characterization (Fig. 4). The sequence-specific assignment was performed with the use of standard triple resonance NMR experiments to obtain the structure at atomic resolution. The structure of the FNIII2 domain was calculated using 778 intra-residual and sequential restraints, 108 medium-range and 772 long-range distance restraints, and 136 backbone torsion angle restraints (Table 2). The calculated

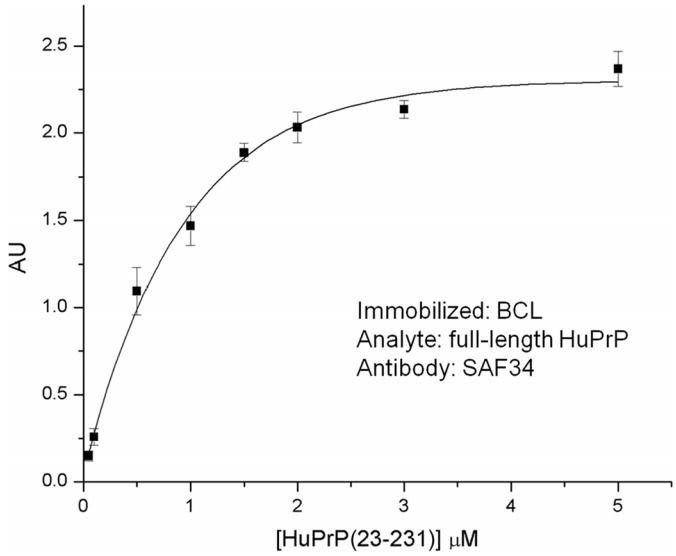

FIGURE 3. **ELISA showing the interaction between BCL peptide (620-NLIKQDDGGSPIRHYL-635) and full-length HuPrP.** *AU*, arbitrary units. *Error bars* indicate ± S.E.

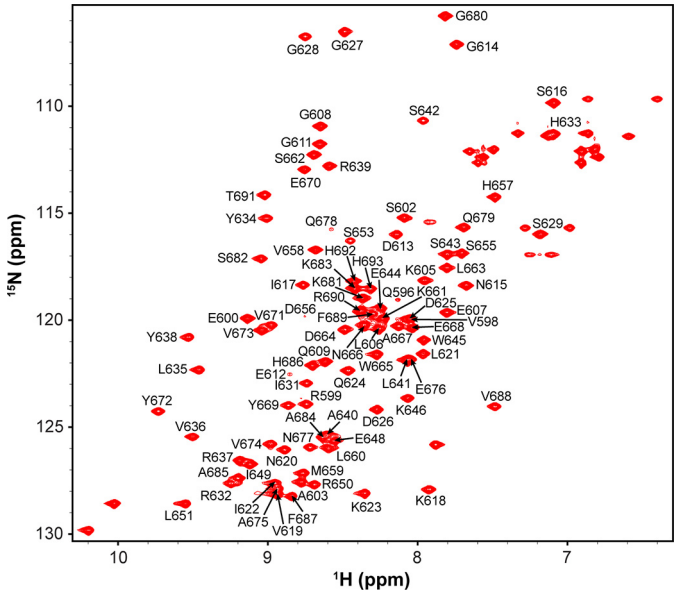

FIGURE 4. **^{15}N HSQC spectrum of FNIII2 domain with assignment of backbone amino acid residues indicated.**

three-dimensional model showed that the FNIII2 domain consists of six antiparallel β-strands, marked *A*–*F* on Fig. 5. They are arranged into two right-handed β-sheets that form a β-sandwich. The first β-sheet is composed of strands A and D (residues Ser^{616}–Asn^{620} and His^{657}–Lys^{661}, respectively), whereas the second β-sheet is composed of strands B, C, E, and F (residues Ile^{631}–Ala^{640}, Ile^{649}–Pro^{652}, Tyr^{669}–Asn^{677}, and Ala^{685}–Phe^{687}, respectively).

NMR approaches of biomolecular complexes are usually challenging because of the increase of molecular weight due to the interaction between partners. Clearly, a large number of similar cross-peaks will be observed and will result in the overlapped spectra and increased linewidths associated with the slower tumbling of a high molecular mass complex. Note that increased line widths of cross-peaks are also expected in the

TABLE 2

NMR restraints and structural statistics for the ensemble of 20 lowest-energy structures of the FNIII2 domain

NOE upper distance limits[a]	
Total	1658
Intra-residue ($\|i-j\|=0$)	337
Sequential ($\|i-j\|=1$)	441
Medium-range ($1<\|i-j\|<5$)	108
Long-range ($\|i-j\|>=5$)	772
Torsion angle restraints	
Backbone (φ/ψ)	136
RMSD to the mean coordinates (Å)	
Ordered backbone atoms (595–691)	0.28 ± 0.09
Ordered heavy atoms (595–691)	0.78 ± 0.08
Ramachandran plot (595–691)[b]	
Residues in most favored regions (%)	88.8
Residues in additional allowed regions (%)	11.2
Structure *Z*-scores[b]	
1st generation packing quality	−0.419 ± 0.568
2nd generation packing quality	7.386 ± 2.149
Ramachandran plot appearance	−3.376 ± 0.339
χ-1/χ-2 rotamer normality	−6.283 ± 0.259
Backbone conformation	−0.441 ± 0.137
RMS *Z*-scores[b]	
Bond lengths	1.201 ± 0.004
Bond angles	0.581 ± 0.008
ω angle restraints	0.758 ± 0.030
Side chain planarity	0.437 ± 0.029
Improper dihedral distribution	0.779 ± 0.016
Inside/Outside distribution	1.029 ± 0.011

[a] None of the 20 structures exhibit distance violations over 0.2 Å and torsion angle violation over 5°.

[b] Ensemble of structures was analyzed by the PROCHECK-NMR and WhatIF programs incorporated in the CING structure evaluation package (54) and PSVS (55).

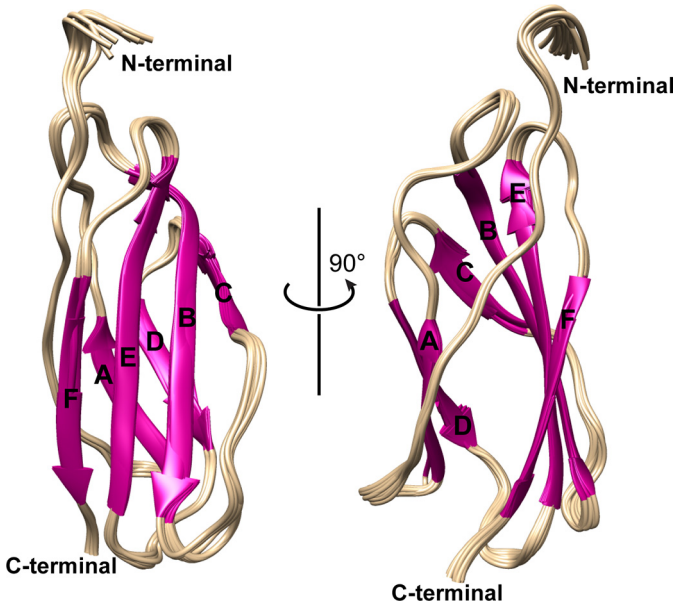

FIGURE 5. **Ensemble of 20 lowest-energy structures of FNIII2 domain (residues 595–691).** The β-strands are highlighted using letter codes (Protein Data Bank ID 5LKN).

spectrum. Moreover, sometimes, macromolecular interactions lead to several line broadenings through the enhanced relaxation that resulted in decrease and even loss of cross-peaks of interest (35, 36). Multidimensional heteronuclear NMR experiments were used to evaluate binding properties between the FNIII2 domain and N-terminal HuPrP(23–144). Interestingly, no amide chemical shift changes (Δδ(H,N)) were observed in the ^{15}N HSQC spectrum of the FNIII2

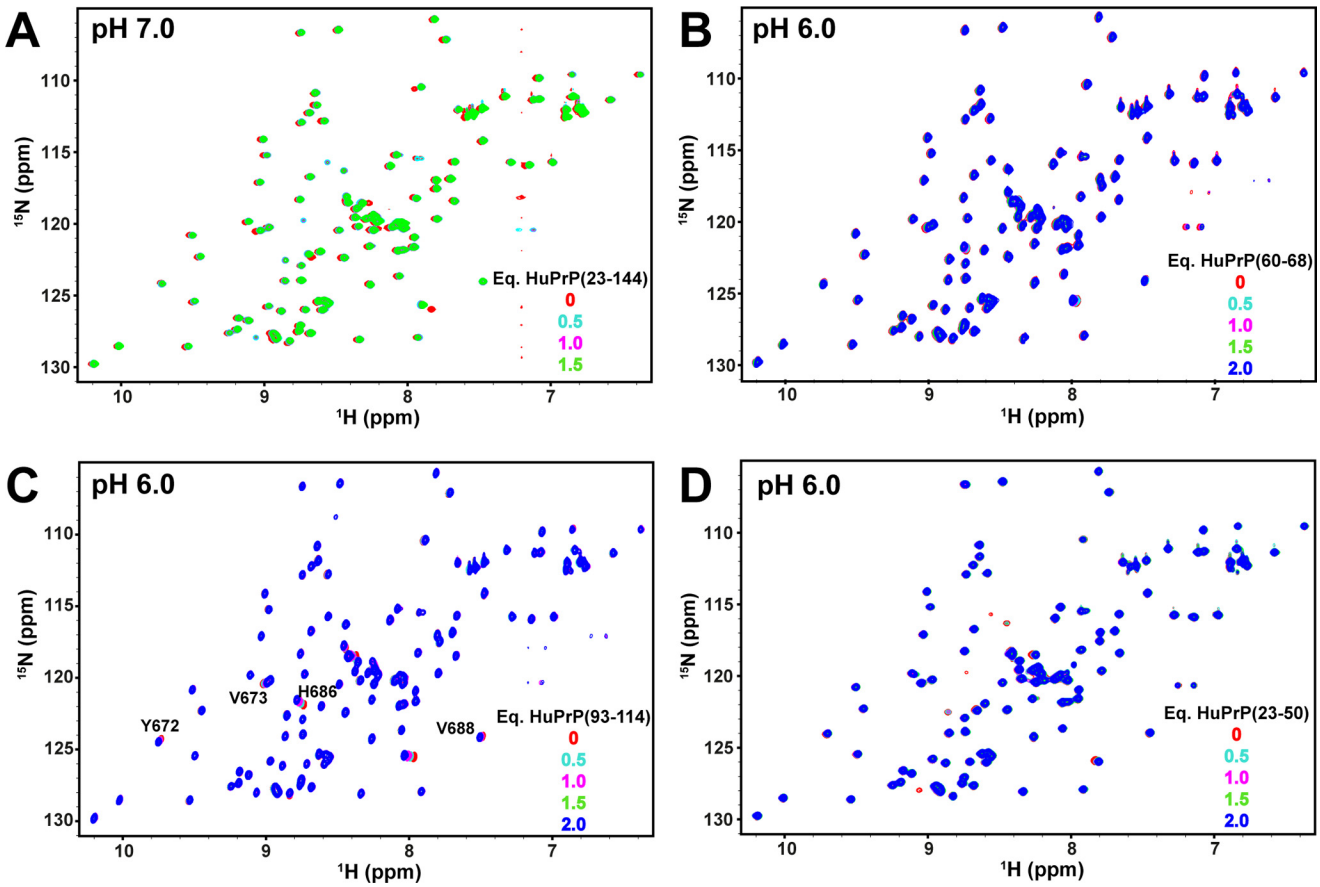

FIGURE 6. **^{15}N HSQC spectra of FNIII2 domain overlaid with ^{15}N HSQC spectra of FNIII2 domain titrated with peptides originating from HuPrP.** *A*, HuPrP(23–144). *B*, HuPrP(60–68). *C*, HuPrP(93–114), HuPrP(93–114). *D*, HuPrP(23–50). The HuPrP peptide to FNIII2 equivalents and pH values are indicated with the corresponding spectra.

domain during a titration experiment with HuPrP(23–144) at pH 7.0 (Fig. 6*A*). However, the FNIII2 sample became blurred upon rising concentration of HuPrP(23–144), presumably because of interactions between partners that also led to insoluble aggregates. Analysis of cross-peak linewidths and absence of chemical shift changes in the ^{15}N HSQC spectra of FNIII2 resulted in the conclusion that cross-peaks correspond to the unbound state of the labeled FNIII2 domain. Additionally, we tried to thermally disrupt multimeric complex at 45 °C to gain the monomeric form of the complex. Although the sample cleared up, indicating that the multimers fell apart, the ^{15}N HSQC spectrum did not improve after thermal treatment. Certainly, even smaller multimeric complexes were still too big to be observed by NMR. Titration was replicated at pH 6. The pH was decreased to achieve favorable conditions where the complex would not precipitate and would be stable often enough that we could observe chemical shift changes of the recorded the ^{15}N HSQC spectra of FNIII2 upon rising concentration of HuPrP peptides. Δδ(H,N) were observed in the ^{15}N HSQC spectra of the FNIII2 domain at a ratio 1:0.5 for residues Arg^{599}, Glu^{600}, Gly^{614}, Arg^{639}, Ser^{642}, Asp^{656}, Ser^{664}, Tyr^{669}, Tyr^{672}, Gln^{678}, Lys^{683}, His^{686}, and Val^{688} (Fig. 7*A*). However, the cross-peaks in the ^{15}N HSQC spectra of the FNIII2 domain disappeared at the ratio 1:2, most likely because of the stacking and forming of aggregates, similarly as observed at higher pH.

Interactions between FNIII2 Domain and Peptides Originate from HuPrP N Terminus—To determine the epitope on HuPrP, its N-terminal part was divided into smaller fragments. Gradual titrations of the FNIII2 domain with individual peptides HuPrP(23–89), HuPrP(23–50), HuPrP(60–68), HuPrP(93–114), and HuPrP(93–114, P102L) were performed to the final ratio between the protein and peptides of 1:2. Upon titrations with HuPrP(23–89), HuPrP(93–114), and HuPrP(93–114, P102L), the Δδ(H,N) values were observed in the ^{15}N HSQC spectra of the FNIII2 domain (Figs. 6*C* and 7, *B* and *C*). In contrast, we did not identify any Δδ(H,N) values of the FNIII2 domain with peptide HuPrP(60–68) and negligible ones with peptide HuPrP(23–50) (Fig. 6, *B* and *D*, respectively). For all titration studies, the Δδ(H,N) values of the FNIII2 domain were calculated using Equation 1 (see "Experimental Procedures"). Titrations with peptides HuPrP(23–144), HuPrP(23–89), and HuPrP(93–114, P102L) resulted in the biggest Δδ(H,N) values of the FNIII2 domain. Interestingly, the biggest Δδ(H,N) values were observed for residues Tyr^{669}, Val^{673}, His^{686}, Phe^{687}, and Val^{688} of the FNIII2 domain. Other cross-peaks of the FNIII2 domain exhibit negligible chemical shift changes. Detailed analysis of the Δδ(H,N) values for the FNIII2 domain presented in Fig. 8 led us to conclude that residues Tyr^{669}, Val^{673}, His^{686},

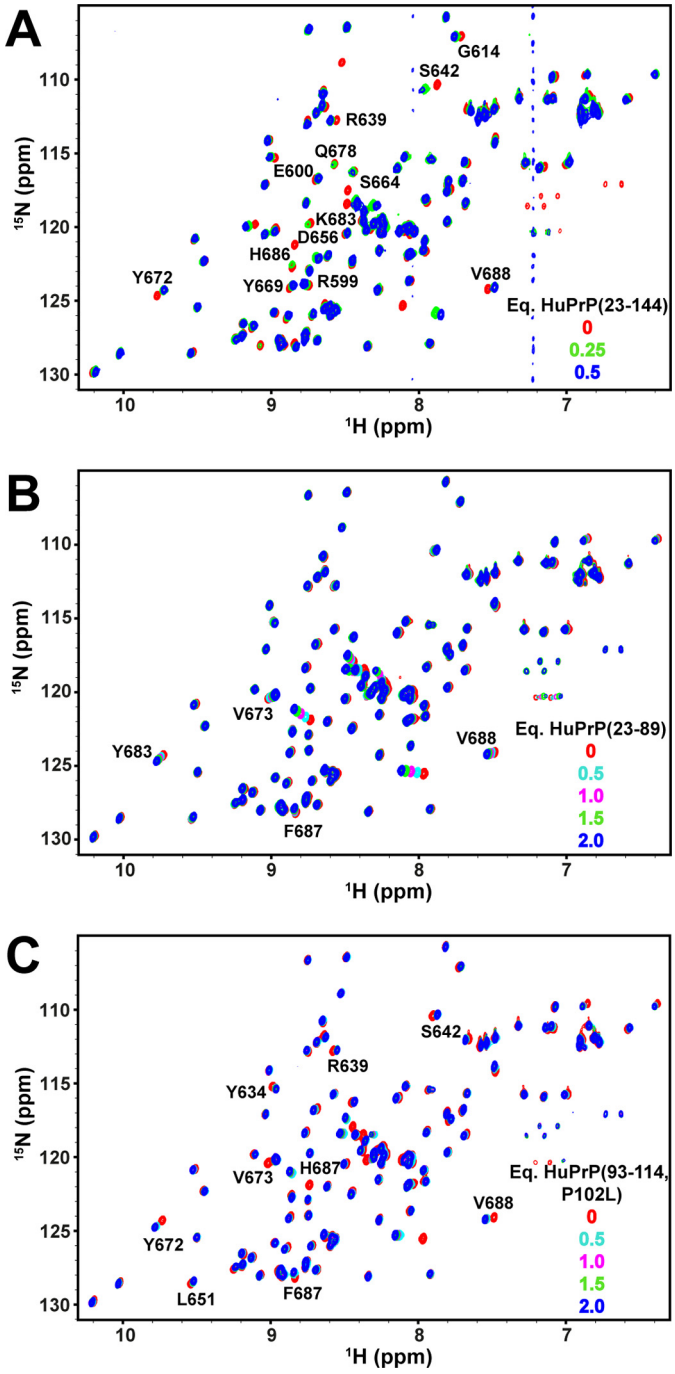

FIGURE 7. **Overlays of ^{15}N HSQC spectra of FNIII2 domain in the presence of peptides originating from HuPrP at pH 6.** *A*, HuPrP(23–144). *B*, HuPrP(23–89). *C*, HuPrP(93–114, P102L). The HuPrP peptide to FNIII2 equivalents are indicated with the corresponding spectra.

Phe^{687}, and Val^{688} of the FNIII2 domain are involved in the interaction with HuPrP.

Interactions between FNIII2 Domain and HuPrP(93–114, P102L)—Because peptide HuPrP(93–114, P102L) exhibited the strongest interactions with the FNIII2 domain, we examined the effects of the interaction on the peptide as well. The ^{15}N HSQC, NOESY, TOCSY, and ^{13}C HSQC spectra of aliphatic and aromatic regions were used for chemical shift assignment of unlabeled peptide. ^{13}C-^{15}N ω_1-filtered 2D NOESY/TOCSY and ^{13}C-^{15}N ω_1-filtered 3D ^{15}N HSQC-NOESY were used to determine inter- and intramolecular contacts in complex. Upon binding, no intermolecular contacts were observed in ^{13}C-^{15}N ω_1-filtered 2D NOESY. The largest intramolecular chemical shift changes were observed for cross-peaks in ^{13}C-^{15}N ω_1-filtered 2D TOCSY of amino acids Trp^{99}, His^{111}, Met^{112}, and Ala^{113} of HuPrP(93–114, P102L).

Experimental data therefore indicate that amino acid residues Tyr^{669}, Val^{673}, His^{686}, Phe^{687}, and Val^{688} of the FNIII2 domain and Trp^{99}, His^{111}, Met^{112}, and Ala^{113} of HuPrP(93–114, P102L) are most probably involved in the interaction of the NCAM domain and WT HuPrP. These data were used as docking restraints for HADDOCK calculation (37, 38). 131 lowest-energy structures were grouped into 13 clusters according to RMSD values. The numbers of structures in the 10 best clusters varied from 4 to 34 with their HADDOCK scores ranging from 71.8 to 53.5. The clusters could be split into two groups of similar size. The first model describes the interactions between Trp^{99} on HuPrP(93–114, P102L) and the FNIII2 domain, whereas the second one describes the interactions of His^{111}–Ala^{113} with HuPrP(93–114, P102L) and the FNIII2 domain (Fig. 9).

Discussion

Among the variety of PrP^C protein interactors (37), PrP^C associates with NCAM *in vivo*. Both molecules have been independently implicated in nervous system development and may play a role in neural stem cells (9, 38, 40). PrP^C recruits to and stabilizes the transmembrane NCAM isoforms (NCAM-180 and NCAM-140) in lipid-rich microdomains. This activates FYN kinase and promotes neurite outgrowth by *cis* and *trans* interactions (13, 41). The interaction of these two molecules and their relation to specific signaling pathways during neurodevelopment merits further investigation at the structural and molecular level, not the least because the physiological role of PrP^C may provide novel insights into the neuropathology of prion diseases.

Along this line, the structural basis of the cross-talk between PrP^C and NCAM has not been previously investigated. In this study, we have performed a structural investigation on the interaction between the recombinant FNIII2 domain of NCAM and different peptides originating from N-terminal human PrP^C using different experimental approaches.

The *in vitro* experiments designed to confirm the co-localization of PrP^C and NCAM in hippocampal neuron cultures led us toward a better understanding of this interaction. We have identified the HuPrP and MoPrP segments able to interact with the FNIII1,2 domain by means of SPR experiments. These experiments have unveiled that the N-terminal HuPrP domain mediates the FNIII1,2 domain binding with high affinity.

X-ray approaches have been previously applied to better understand the structural properties of the FNIII1,2 domain (42). Interestingly, the comparison between the FNIII2 NMR structure and the corresponding x-ray structure revealed local structural differences in the length of β-strands. In particular, although the NMR structure features two short β-strands (A and D) on one protein side and four β-strands (B, C, E, and F) on the other, the x-ray structure is characterized by seven

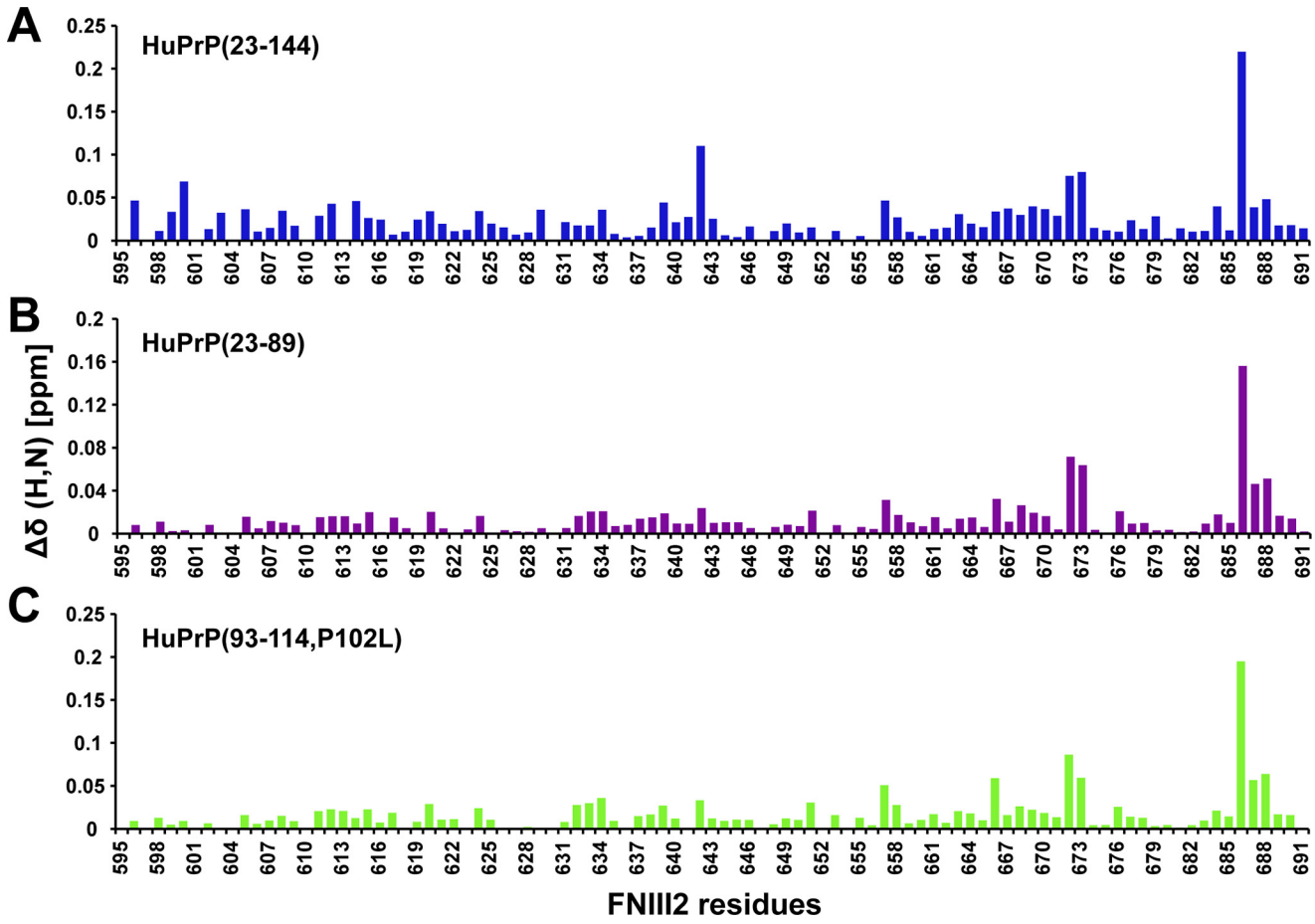

FIGURE 8. **Chemical shift changes Δδ(H,N) for FNIII2 domain upon interaction with peptides originating from HuPrP at pH 6. 0.** *A*, HuPrP(23–144) peptide at ratio 1:0.5. *B*, HuPrP(93–114, P102L) at ratio 1:2. *C*, HuPrP(23–89) at ratio 1:2. The Δδ(H,N) values were calculated using Equation 1 (see "Experimental Procedures").

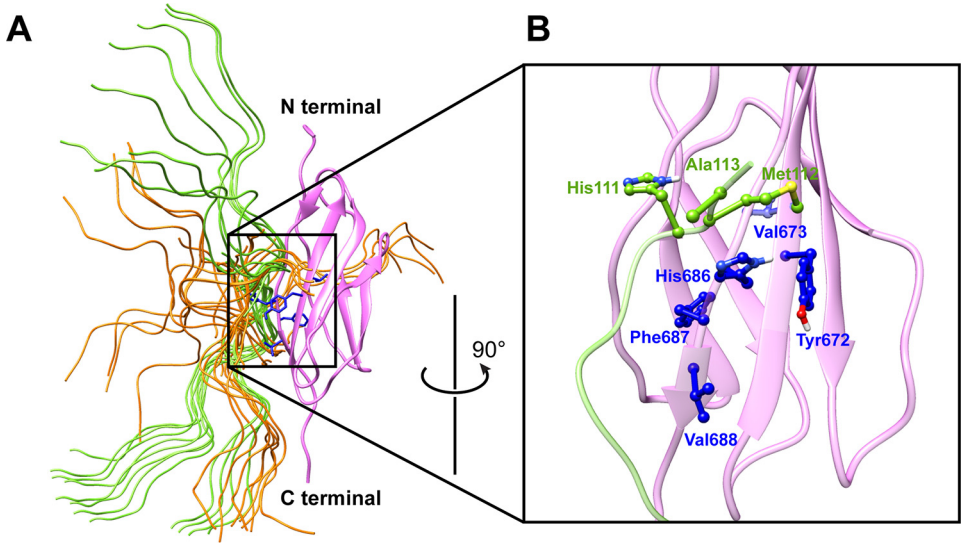

FIGURE 9. **Low-resolution model of complex between FNIII2 domain and HuPrP(93–114, P102L).** *A*, ensemble of 40 models of the complex between the FNIII2 domain (*pink*) and HuPrP(93–114, P102L) (*green* or *orange* depending on whether it interacts with His^{111}–Ala^{113} or Trp^{99}, respectively) clustered by the HADDOCK program (4 models from each of 10 clusters). *B*, enlarged binding region of the best HADDOCK model of the FNIII2 domain-HuPrP(93–114, P102L) complex. Amino acids involved in the interaction are presented with balls and sticks (FNIII2 domain in *blue*, HuPrP(93–114, P102L) in *green*).

β-strands (supplemental Fig. S2). Structural discrepancies between diffraction and NMR data are to be expected considering the differences of the two methods in terms of spatial distribution of the molecules in the sample and time scales accessible to each method. Notably, solution NMR data represent an average over semi-randomly oriented mol-

ecules in solution detected in a nanosecond-to-second time regime, whereas diffraction data represent an average over molecules arranged in a periodic crystal lattice acquired in a seconds time scale.

We have performed NMR experiments designed to identify the binding sites on the FNIII2 domain and HuPrP N terminus responsible for the interaction. The implications of our findings are important in prion biology as we provide the first structural evidence that NCAM mediates the interaction with the N-terminal domain of HuPrP through its FNIII1,2 domain. We propose a model where this largely unstructured segment acts as a dynamic element able to recruit NCAM molecules and to mediate physiological processes. We found that the WT HuPrP mediates binding with the FNIII2 domain via its N-terminal segment (residues 23–144). Interestingly, the N terminus contains a glycosaminoglycan (GAG)-binding motif. The binding of GAG is important in prion diseases. This idea is supported by evidence that mutant recombinant PrP binds more GAG, which promotes the aggregation of mutant recombinant PrP more efficiently than HuPrP wild type (43). Thus, our present data corroborate the idea that besides binding metal ions and GAG, the N-terminal domain also mediates *cis* interactions with the NCAM fibronectin domain.

As opposed to WT HuPrP, the P102L mutant seems to possess an extra binding site localized in the segment 93–114, also denoted as the non-octarepeat copper-binding site (32, 44). Peptides HuPrP(93–114) and HuPrP(93–114, P102L) have the same position in HuPrP N terminus except for the proline-to-leucine substitution at residue 102. Comparison of the $\Delta\delta$(H,N) values for the FNIII2 domain after titration with both HuPrP(93–114) and HuPrP(93–114, P102L) led to a conclusion that the interaction of the latter with the FNIII2 domain is stronger. Thus, we argue that P102L mutation may affect binding with the FNIII2 domain, presumably leading to a stronger interaction with NCAM, which in turn may lead to abnormal Src family kinase activation.

These findings about the interaction between HuPrP and NCAM may have biological relevance on prion conversion. Different compounds, including antibodies or chemical drugs, with high affinity for PrP^C have been employed as candidates for therapeutic approaches aimed at inhibiting prion replication. This approach postulates that any PrP^C ligand acts as molecular chaperone able to stabilize the protein folding, thus limiting the conversion to PrP^{Sc}. NCAM does not play a direct role during prion formation as observed in NCAM knock-out mice showing the same incubation period when compared with wild-type mice infected by prions (21). It is plausible that any interference with NCAM-mediated signaling in the diseased brain may favor cell death and inhibit synaptic plasticity. The interactions between PrP^C and NCAM could therefore be reduced by accumulation of PrP^{Sc} in the diseased nervous system. Thus, it is conceivable that the association of NCAM to PrP^C favors functional signaling pathways through FYN, which is also implicated in synaptic functions. Furthermore, PrP^C-NCAM crosstalk is crucial for the coordinated regulation of cell cycle progression and the differentiation of neuronal precursors toward different neuronal phenotypes (40). We found that this interaction is mediated by the PrP^C N terminus, particularly in the segment from residues 23 to 50. This includes four positively charged residues (*i.e.* KKRPK) known to play a role in the PrP^C endocytic trafficking and in its localization to lipid rafts (45, 46). Our study suggests that the interaction between residues 23–50 and the NCAM fibronectin domain may determine the fate of PrP^C in the cell surface raft domain. Here PrP^C participates in the complex molecular networks and signaling mechanisms, both cell-intrinsic and cell-extrinsic, that influence cell fate and differentiation.

The mechanisms that recruit and assemble different transmembrane signaling molecules to distinct membrane subdomains have only started to emerge. In these environments, signaling and scaffolding proteins can self-associate and form dimeric or multimeric assemblies. Protein dimerization has been reported as a common mechanism to cluster downstream signaling components and thereby enhance the signaling cascade (47). According to a recent model, NCAM is present on the cell surface as *cis* dimers, formed by the interactions between the Ig1 and Ig2 domains (48, 49). The role of *cis* dimerization in NCAM dimerization is debated, but it is a prerequisite for NCAM clustering on the cell surface, which in turn results in cell-cell adhesion via *trans* interactions between NCAM clusters.

We described a strong interaction between HuPrP N terminus and FNIII1,2 and the formation of multimeric complexes formed upon the addition of FNIII2 to HuPrP(23–144). This may have important physiological implications as PrP^C may act as a scaffolding protein able to facilitate the FNIII1,2-mediated NCAM self-assembly and clustering in the lipid raft.

In conclusion, we provide structural evidence that NCAM mediates a heterophilic interaction through FNIII1,2 and the N-terminal domain of HuPrP. Importantly, we propose that this largely unstructured segment acts as dynamic element able to recruit NCAM molecules and to mediate physiological processes.

Experimental Procedures

Cell Culture—P1-P2 FVB WT mice were sacrificed by decapitation in accordance with the guidelines of the Italian Animal Welfare Act.

Immunostaining—Cells were fixed in 4% paraformaldehyde containing 0.15% picric acid in PBS, saturated with 0.1 M glycine, permeabilized with 0.1% Triton X-100, saturated with 0.5% BSA (all from Sigma-Aldrich) in PBS, and then incubated for 1 h with primary antibodies followed by a 30-min incubation with secondary antibodies conjugated with STAR580 or STAR635P (Abberior, Göttingen, Germany). All incubations were performed at room temperature (20–22 °C).

STED Microscopy—Two-color STED microscopy was performed at the NanoBiophotonics Department (Max Plank Institute for Biophysical Chemistry, Göttingen, Germany) (50) equipped with 561- and 640-nm pulsed excitation lasers, a pulsed 775-nm STED laser, and a 100× oil immersion objective lens (NA 1.4).

Plasmid Construction—The FNIII1,2 and FNIII2 domains were PCR-amplified from pCEP-Pu vector encoding for FNIII1,2 (kindly provided by Dr. Federico Carafoli, Imperial College London, London, UK) and inserted into a modified pET11a vector (*i.e.* carrying a C-terminal uncleavable His tag)

TABLE 3
Amino acid sequences of peptides originating from N-terminal HuPrP that were used for characterization of binding properties between HuPrP and NCAM

Names of peptides	Amino acidic sequences
HuPrP(23–144)	KKRPKPGGWNTGGSRYPGQGSPGGNRYPPQGGGGWGQPHGGGWGQPHGGGWGQPHGGGWGQPHG GGWGQGGGTHSQWNKPSKPKTNMKHMAGAAAAGAVVGGLGGYMLGSAMSRPIIHFGSD
HuPrP(23–89)	KKRPKPGGWNTGGSRYPGQGSPGGNRYPPQGGGGWGQPHGGGWGQPHGGGWGQPHGGGW
HuPrP(23–50)	KKRPKPGGWNTGGSRYPGQGSPGGNRYP
HuPrP(93–114)	GGTHSQWNKPSKPKTNMKHMAG
HuPrP(93–114, P102L)	GGTHSQWNKLSKPKTNMKHMAG
HuPrP(60–68)	PHGGGWGQ

using a restriction-free cloning protocol. Our FNIII1,2 and FNIII1 numbering schemes correspond to Carafoli *et al.* (42).

Protein Expression and Purification—A freshly transformed overnight culture of *Escherichia coli* BL21 (DE3) cells (Stratagene) transformed with pET11a encoding for FNIII1,2 or FNIII2 was added at 37 °C to 2 liters of minimal medium. For isotope labeling, 4 g/liter [$^{13}C_6$]glucose and 1 g/liter [^{15}N]ammonium chloride were added. At 0.8 A_{600}, expression was induced with isopropyl-β-D-galactopyranoside to a final concentration of 0.25 mM. Cells were grown in a BIOSTAT B plus 2-liter vessel (Sartorius) and harvested 18 h after inoculation. Bacterial paste was resuspended in 25 mM Tris-HCl, 0.8% Triton X-100, 1 mM PMSF, pH 8, and lysed by a Panda homogenizer. Crude extract was loaded onto a 5-ml HisTrap column (GE Healthcare) equilibrated in PBS buffer, pH 7.45 (140 mM NaCl, 10 mM Na_2PO_4, and 3 mM KCl), and then eluted with 500 mM imidazole in PBS. The protein was then dialyzed against TBS buffer, pH 7.45, using a Spectra/Por membrane (molecular weight, 10,000).

The HuPrP(23–231), HuPrP(90–231), and HuPrP(23–144) were expressed, purified, and *in vitro* refolded according to our previous protocols (32). Peptides HuPrP(23–89), HuPrP(23–50), HuPrP(60–68), HuPrP(93–114), and HuPrP(93–114, P102L) (Table 3) were purchased from Chematek SpA.

NCAM-PrP Affinities Were Determined Using Surface Plasmon Resonance—Binding kinetics were determined on Biacore 2000 (GE Healthcare). Ten μg of NCAM was diluted in 10 mM NaOAc, pH 5.2, and immobilized on a CM5 chip activated with NHS and *N*-ethyl-N-(3-dimethylaminopropyl) carbodiimide (EDC), using a flow rate of 5 μl/min. A steady signal of about 400 response units was obtained after immobilization and blocking with ethanol amine. All kinetic SPR analyses were run at a flow rate of 30 μl/min in PBS, 0.05% Tween 20, and 3 mM EDTA at 25 °C. After each cycle, the surface was regenerated with a 60-s pulse of 100 mM glycine, pH 1.5. Association rates (K_{on}) and dissociation rates (K_{off}) were obtained using a 1:1 Langmuir binding model (Biacore evaluation software version 4.1). The equilibrium dissociation constant (K_d) was calculated from the ratio K_{off}/K_{on}.

Confirming BCL-HuPrP Interaction with ELISA—BCL was immobilized at 0.5 μM and titrated with full-length HuPrP (0–5 μM). Antigen was detected using anti-PrP^C SAF34 antibody that recognizes an epitope corresponding to the octapeptide repeat region (residues 60–91) (51).

NMR Spectroscopy—All NMR experiments used for structure determination were performed on ^{13}C,^{15}N isotopically labeled FNIII2 domain on the Varian VNMRS 800-MHz NMR spectrometer equipped with a triple ^{1}H/^{13}C/^{15}N resonance cryogenic probe head with inverse detection at 298 K. The NMR sample contained 0.9 mM FNIII2 domain in 50 mM TBS buffer, pH 7.45, and 150 mM NaCl. NMR experiments for HN and HC detection were performed in 90%/10% H_2O/D_2O and 100% deuterated buffer, respectively. The sequence-specific assignment of the backbone resonances for the FNIII2 domain was obtained using standard double resonance ^{15}N HSQC and triple resonance NMR experiments HNCO, HN(CO)CA, HNCA, HN(CO)CACB, and HNCACB. ^{1}H and ^{13}C resonances of aliphatic and aromatic side chains were assigned using ^{13}C HSQC and HAHB(CO)NH, CC(CO)NH, (H)CCH-TOCSY, and ^{13}C-edited HSQC-NOESY experiments. NOE contacts were determined in 3D ^{15}N- and ^{13}C-edited HSQC-NOESY experiments to perform structure calculation. The structure modeling of the FNIII2 domain was performed using the program CYANA 3.0 (52). Structure refinement using the explicit solvent model was performed by the YASARA program (53). An ensemble of 20 lowest-energy structures of the FNIII2 domain was validated by the web server software ICing (54) and PSVS (55).

Titration of ^{13}C,^{15}N isotopically labeled FNIII2 domain with unlabeled HuPrP(23–144) was performed in 25 mM HEPES buffer, pH 7.00. Titrations of labeled FNIII2 domain were also done with unlabeled HuPrP(23–50), HuPrP(23–89), HuPrP(60–68), HuPrP(93–114), and HuPrP(93–114, P102L) peptides at pH 6.00 (20 mM NaOAc buffer, 0.35 mM labeled FNIII2 domain per titration experiment). Titrations were followed by analysis of the $\Delta\delta$(H,N) of the FNIII2 domain in ^{15}N HSQC experiments. All recorded spectra were processed by the NMRPipe (56) software and analyzed with the CARA (57) and SPARKY (58) software.

Amide chemical shift changes were calculated for each non-overlapped cross-peak in the ^{15}N HSQC spectrum of the FNIII2 domain according to Equations 1 and 2

$$\Delta\delta(\mathrm{H,N}) = \sqrt{(\Delta\delta_H)^2 + (0.154 \times \Delta\delta_N)^2} \quad \text{(Eq. 1)}$$

$$\Delta\delta_{H,N} = \delta_{H,N\ bound} - \delta_{H,N\ free} \quad \text{(Eq. 2)}$$

where $\Delta\delta_H$ and $\Delta\delta_N$ are defined as the difference in the ^{1}H and ^{15}N amide chemical shifts between the protein-peptide complex and the free state of the FNIII2 domain (59).

Modeling the Complex between FNIII2 Domain and HuPrP (93–114, P102L)—Modeling of the complex between the FNIII2 domain and HuPrP(93–114, P102L) was made with the HADDOCK software (33, 39).

Author Contributions—U. S., G. S., G. G., G. I., and B. Z. performed the NMR experiments. U. S., G. I., B. Z., I. B., and J. P. analyzed NMR data. G. L., G. S., and G. G. provided protein samples. L. A. performed and analyzed STED nanoscopy experiments. R. N. N. A. performed and analyzed SPR data. U. S., G. S., G. G., and G. L. wrote the paper. G. L., J. P., and G. G. conceived and designed the experiments. All authors read and approved the final manuscript.

Acknowledgments—Access to NMR spectrometers was funded partially through CERIC-ERIC. We acknowledge Dr. Federico Carafoli (Imperial College London, London, UK) for providing the plasmid encoding for FNIII1,2 and Dr. Dan Cojoc (IOM-CNR, Trieste, Italy) for technical support. We are grateful to Jan Steyaert (VUB, Brussels, Belgium) for providing valuable information and suggestions.

Note Added in Proof—Supplemental Fig. S1 was mistakenly duplicated as Fig. 6 in the version of this article published as a Paper in Press on August 17, 2016. This error has now been corrected and does not affect the results or conclusions of this work.

References

1. Colby, D. W., and Prusiner, S. B. (2011) Prions. *Cold Spring Harb. Perspect. Biol.* **3,** a006833
2. Zahn, R., Liu, A., Lührs, T., Riek, R., von Schroetter, C., López García, F., Billeter, M., Calzolai, L., Wider, G., and Wüthrich, K. (2000) NMR solution structure of the human prion protein. *Proc. Natl. Acad. Sci. U.S.A.* **97,** 145–150
3. Prusiner, S. B. (1982) Novel proteinaceous infectious particles cause scrapie. *Science* **216,** 136–144
4. Requena, J. R., and Wille, H. (2014) The structure of the infectious prion protein: experimental data and molecular models. *Prion* **8,** 60–66
5. Collinge, J., Whittington, M. A., Sidle, K. C. L., Smith, C. J., Palmer, M. S., Clarke, A. R., and Jefferys, J. G. R. (1994) Prion protein is necessary for normal synaptic function. *Nature* **370,** 295–297
6. Bremer, J., Baumann, F., Tiberi, C., Wessig, C., Fischer, H., Schwarz, P., Steele, A. D., Toyka, K. V., Nave, K. A., Weis, J., and Aguzzi, A. (2010) Axonal prion protein is required for peripheral myelin maintenance. *Nat. Neurosci.* **13,** 310–318
7. Devanathan, V., Jakovcevski, I., Santuccione, A., Li, S., Lee, H. J., Peles, E., Leshchyns'ka, I., Sytnyk, V., and Schachner, M. (2010) Cellular form of prion protein inhibits Reelin-mediated shedding of Caspr from the neuronal cell surface to potentiate Caspr-mediated inhibition of neurite outgrowth. *J. Neurosci.* **30,** 9292–9305
8. Lee, Y. J., and Baskakov, I. V. (2013) The cellular form of the prion protein is involved in controlling cell cycle dynamics, self-renewal, and the fate of human embryonic stem cell differentiation. *J. Neurochem.* **124,** 310–322
9. Steele, A. D., Emsley, J. G., Ozdinler, P. H., Lindquist, S., and Macklis, J. D. (2006) Prion protein (PrP^c) positively regulates neural precursor proliferation during developmental and adult mammalian neurogenesis. *Proc. Natl. Acad. Sci. U.S.A.* **103,** 3416–3421
10. Maglio, L. E., Perez, M. F., Martins, V. R., Brentani, R. R., and Ramirez, O. A. (2004) Hippocampal synaptic plasticity in mice devoid of cellular prion protein. *Brain Res. Mol. Brain Res.* **131,** 58–64
11. Caiati, M. D., Safiulina, V. F., Fattorini, G., Sivakumaran, S., Legname, G., and Cherubini, E. (2013) PrP^C controls via protein kinase A the direction of synaptic plasticity in the immature hippocampus. *J. Neurosci.* **33,** 2973–2983
12. Mouillet-Richard, S., Ermonval, M., Chebassier, C., Laplanche, J. L., Lehmann, S., Launay, J. M., and Kellermann, O. (2000) Signal transduction through prion protein. *Science* **289,** 1925–1928
13. Santuccione, A., Sytnyk, V., Leshchyns'ka, I., and Schachner, M. (2005) Prion protein recruits its neuronal receptor NCAM to lipid rafts to activate $p59^{fyn}$ and to enhance neurite outgrowth. *J. Cell Biol.* **169,** 341–354
14. Gasperini, L., Meneghetti, E., Pastore, B., Benetti, F., and Legname, G. (2015) Prion protein and copper cooperatively protect neurons by modulating NMDA receptor through *S*-nitrosylation. *Antioxid. Redox Signal.* **22,** 772–784
15. Khosravani, H., Zhang, Y., Tsutsui, S., Hameed, S., Altier, C., Hamid, J., Chen, L., Villemaire, M., Ali, Z., Jirik, F. R., and Zamponi, G. W. (2008) Prion protein attenuates excitotoxicity by inhibiting NMDA receptors. *J. Cell Biol.* **181,** 551–565
16. Pushie, M. J., Pickering, I. J., Martin, G. R., Tsutsui, S., Jirik, F. R., and George, G. N. (2011) Prion protein expression level alters regional copper, iron and zinc content in the mouse brain. *Metallomics* **3,** 206–214
17. Santos, T. G., Silva, I. R., Costa-Silva, B., Lepique, A. P., Martins, V. R., and Lopes, M. H. (2011) Enhanced neural progenitor/stem cells self-renewal via the interaction of stress-inducible protein 1 with the prion protein. *Stem Cells* **29,** 1126–1136
18. Gauczynski, S., Peyrin, J. M., Haïk, S., Leucht, C., Hundt, C., Rieger, R., Krasemann, S., Deslys, J. P., Dormont, D., Lasmézas, C. I., and Weiss, S. (2001) The 37-kDa/67-kDa laminin receptor acts as the cell-surface receptor for the cellular prion protein. *EMBO J.* **20,** 5863–5875
19. Hajj, G. N. M., Lopes, M. H., Mercadante, A. F., Veiga, S. S., da Silveira, R. B., Santos, T. G., Ribeiro, K. C. B., Juliano, M. A., Jacchieri, S. G., Zanata, S. M., and Martins, V. R. (2007) Cellular prion protein interaction with vitronectin supports axonal growth and is compensated by integrins. *J. Cell Sci.* **120,** 1915–1926
20. Schmitt-Ulms, G., Hansen, K., Liu, J., Cowdrey, C., Yang, J., DeArmond, S. J., Cohen, F. E., Prusiner, S. B., and Baldwin, M. A. (2004) Time-controlled transcardiac perfusion cross-linking for the study of protein interactions in complex tissues. *Nat. Biotechnol.* **22,** 724–731
21. Schmitt-Ulms, G., Legname, G., Baldwin, M. A., Ball, H. L., Bradon, N., Bosque, P. J., Crossin, K. L., Edelman, G. M., DeArmond, S. J., Cohen, F. E., and Prusiner, S. B. (2001) Binding of neural cell adhesion molecules (N-CAMs) to the cellular prion protein. *J. Mol. Biol.* **314,** 1209–1225
22. Watts, J. C., Huo, H., Bai, Y., Ehsani, S., Jeon, A. H. W., Won, A. H., Shi, T., Daude, N., Lau, A., Young, R., Xu, L., Carlson, G. A., Williams, D., Westaway, D., and Schmitt-Ulms, G. (2009) Interactome analyses identify ties of PrP and its mammalian paralogs to oligomannosidic *N*-glycans and endoplasmic reticulum-derived chaperones. *PLoS Pathog.* **5,** e1000608
23. Mehrabian, M., Brethour, D., Wang, H., Xi, Z., Rogaeva, E., and Schmitt-Ulms, G. (2015) The Prion protein controls polysialylation of neural cell adhesion molecule 1 during cellular morphogenesis. *PLoS One* **10,** e0133741
24. Crossin, K. L., and Krushel, L. A. (2000) Cellular signaling by neural cell adhesion molecules of the immunoglobulin superfamily. *Dev. Dyn.* **218,** 260–279
25. Schachner, M. (1997) Neural recognition molecules and synaptic plasticity. *Curr. Opin. Cell Biol.* **9,** 627–634
26. Boutin, C., Schmitz, B., Cremer, H., and Diestel, S. (2009) NCAM expression induces neurogenesis *in vivo*. *Eur. J. Neurosci.* **30,** 1209–1218
27. Frei, T., von Bohlen und Halbach, F., Wille, W., and Schachner, M. (1992) Different extracellular domains of the neural cell adhesion molecule (N-CAM) are involved in different functions. *J. Cell Biol.* **118,** 177–194
28. Soroka, V., Kasper, C., and Poulsen, F. M. (2010) Structural biology of NCAM. in *Structure and Function of the Neural Cell Adhesion Molecule NCAM* (Berezin, V., ed), pp 3–22, Springer New York
29. Kiselyov, V. V., Skladchikova, G., Hinsby, A. M., Jensen, P. H., Kulahin, N., Soroka, V., Pedersen, N., Tsetlin, V., Poulsen, F. M., Berezin, V., and Bock, E. (2003) Structural basis for a direct interaction between FGFR1 and NCAM and evidence for a regulatory role of ATP. *Structure* **11,** 691–701
30. Kiselyov, V. V., Soroka, V., Berezin, V., and Bock, E. (2005) Structural biology of NCAM homophilic binding and activation of FGFR. *J. Neurochem.* **94,** 1169–1179
31. Taubner, L. M., Bienkiewicz, E. A., Copié, V., and Caughey, B. (2010) Structure of the flexible amino-terminal domain of prion protein bound to a sulfated glycan. *J. Mol. Biol.* **395,** 475–490
32. Giachin, G., Mai, P. T., Tran, T. H., Salzano, G., Benetti, F., Migliorati, V., Arcovito, A., Della Longa, S., Mancini, G., D'Angelo, P., and Legname, G. (2015) The non-octarepeat copper binding site of the prion protein is a key regulator of prion conversion. *Sci. Rep.* **5,** 15253

33. Wassenaar, T. A., van Dijk, M., Loureiro-Ferreira, N., van der Schot, G., de Vries, S. J., Schmitz, C., van der Zwan, J.., Boelens, R., Giachetti, A., Ferella, L., Rosato, A., Bertini, I., Herrmann, T., Jonker, H. R. A., Bagaria, A., *et al.* (2012) WeNMR: structural biology on the grid. *J. Grid Comput.* **10,** 743–767
34. Jacobsen, J., Kiselyov, V., Bock, E., and Berezin, V. (2008) A peptide motif from the second fibronectin module of the neural cell adhesion molecule, NCAM, NLIKQDDGGSPIRHY, is a binding site for the FGF receptor. *Neurochem. Res.* **33,** 2532–2539
35. McElroy, C., Manfredo, A., Wendt, A., Gollnick, P., and Foster, M. (2002) TROSY-NMR studies of the 91 kDa TRAP protein reveal allosteric control of a gene regulatory protein by ligand-altered flexibility. *J. Mol. Biol.* **323,** 463–473
36. Cavanagh, J., Fairbrother, W. J., Palmer III, A. G., and Skelton, N. J. (1995) *Protein NMR Spectroscopy: Principles and Practice*, Academic Press
37. Aguzzi, A., Baumann, F., and Bremer, J. (2008) The prion's elusive reason for being. *Annu. Rev. Neurosci.* **31,** 439–477
38. Amoureux, M. C., Cunningham, B. A., Edelman, G. M., and Crossin, K. L. (2000) N-CAM binding inhibits the proliferation of hippocampal progenitor cells and promotes their differentiation to a neuronal phenotype. *J. Neurosci.* **20,** 3631–3640
39. de Vries, S. J., van Dijk, M., and Bonvin, A. M. J. J. (2010) The HADDOCK web server for data-driven biomolecular docking. *Nat. Protoc.* **5,** 883–897
40. Prodromidou, K., Papastefanaki, F., Sklaviadis, T., and Matsas, R. (2014) Functional cross-talk between the cellular prion protein and the neural cell adhesion molecule is critical for neuronal differentiation of neural stem/precursor cells. *Stem Cells* **32,** 1674–1687
41. Bodrikov, V., Leshchyns'ka, I., Sytnyk, V., Overvoorde, J., den Hertog, J., and Schachner, M. (2005) RPTPα is essential for NCAM-mediated p59^{fyn} activation and neurite elongation. *J. Cell Biol.* **168,** 127–139
42. Carafoli, F., Saffell, J. L., and Hohenester, E. (2008) Structure of the tandem fibronectin type 3 domains of neural cell adhesion molecule. *J. Mol. Biol.* **377,** 524–534
43. Silva, J. L., Vieira, T. C., Gomes, M. P., Rangel, L. P., Scapin, S. M., and Cordeiro, Y. (2011) Experimental approaches to the interaction of the prion protein with nucleic acids and glycosaminoglycans: modulators of the pathogenic conversion. *Methods* **53,** 306–317
44. D'Angelo, P., Della Longa, S., Arcovito, A., Mancini, G., Zitolo, A., Chillemi, G., Giachin, G., Legname, G., and Benetti, F. (2012) Effects of the pathological Q212P mutation on human prion protein non-octarepeat copper-binding site. *Biochemistry* **51,** 6068–6079
45. Taylor, D. R., Watt, N. T., Perera, W. S. S., and Hooper, N. M. (2005) Assigning functions to distinct regions of the N-terminus of the prion protein that are involved in its copper-stimulated, clathrin-dependent endocytosis. *J. Cell Sci.* **118,** 5141–5153
46. Walmsley, A. R., Zeng, F., and Hooper, N. M. (2003) The N-terminal region of the prion protein ectodomain contains a lipid raft targeting determinant. *J. Biol. Chem.* **278,** 37241–37248
47. Marianayagam, N. J., Sunde, M., and Matthews, J. M. (2004) The power of two: protein dimerization in biology. *Trends Biochem. Sci.* **29,** 618–625
48. Kulahin, N., Grunnet, L. G., Lundh, M., Christensen, D. P., Jorgensen, R., Heding, A., Billestrup, N., Berezin, V., Bock, E., and Mandrup-Poulsen, T. (2011) Direct demonstration of NCAM *cis*-dimerization and inhibitory effect of palmitoylation using the BRET2 technique. *FEBS Lett.* **585,** 58–64
49. Soroka, V., Kolkova, K., Kastrup, J. S., Diederichs, K., Breed, J., Kiselyov, V. V., Poulsen, F. M., Larsen, I. K., Welte, W., Berezin, V., Bock, E., and Kasper, C. (2003) Structure and interactions of NCAM Ig1–2-3 suggest a novel zipper mechanism for homophilic adhesion. *Structure* **11,** 1291–1301
50. Göttfert, F., Wurm, C. A., Mueller, V., Berning, S., Cordes, V. C., Honigmann, A., and Hell, S. W. (2013) Coaligned dual-channel STED nanoscopy and molecular diffusion analysis at 20 nm resolution. *Biophys. J.* **105,** L01–03
51. Perrier, V., Solassol, J., Crozet, C., Frobert, Y., Mourton-Gilles, C., Grassi, J., and Lehmann, S. (2004) Anti-PrP antibodies block PrP^{Sc} replication in prion-infected cell cultures by accelerating PrP^C degradation. *J. Neurochem.* **89,** 454–463
52. Güntert, P. (2004) Automated NMR structure calculation with CYANA. *Methods Mol. Biol.* **278,** 353–378
53. Krieger, E., Koraimann, G., and Vriend, G. (2002) Increasing the precision of comparative models with YASARA NOVA: a self-parameterizing force field. *Proteins* **47,** 393–402
54. Doreleijers, J. F., Sousa da Silva, A. W., Krieger, E., Nabuurs, S. B., Spronk, C. A. E. M., Stevens, T. J., Vranken, W. F., Vriend, G., and Vuister, G. W. (2012) CING: an integrated residue-based structure validation program suite. *J. Biomol. NMR* **54,** 267–283
55. Bhattacharya, A., Tejero, R., and Montelione, G. T. (2007) Evaluating protein structures determined by structural genomics consortia. *Proteins* **66,** 778–795
56. Delaglio, F., Grzesiek, S., Vuister, G. W., Zhu, G., Pfeifer, J., and Bax, A. (1995) NMRPipe: a multidimensional spectral processing system based on UNIX pipes. *J. Biomol. NMR* **6,** 277–293
57. Keller, R. L. J. (2004) *The Computer Aided Resonance Assignment Tutorial*, Institute for Molecular Biology and Biophysics, The Swiss Federal Institute of Technology, Zurich, Switzerland
58. Goddard, T. D., and Kneller, D. G. (2008) *SPARKY 3*, University of California, San Francisco
59. Mulder, F. A., Schipper, D., Bott, R., and Boelens, R. (1999) Altered flexibility in the substrate-binding site of related native and engineered high-alkaline *Bacillus* subtilisins. *J. Mol. Biol.* **292,** 111–123